CHEMISTRY
A EUROPEAN JOURNAL

Discrepancy between the Spin Distribution and the Magnetic Ground State for a Triaminoxyl Substituted Triphenylphosphine Oxide Derivative

Oscar Benedi Borobia,[a] Philippe Guionneau,[a] Henrike Heise,[b, f] Frank H. Köhler,*[b] Laurent Ducasse,[c] Jose Vidal-Gancedo,[d] Jaume Veciana,*[d] Stéphane Golhen,[e] Lahcène Ouahab,[e] and Jean-Pascal Sutter*[a]

Abstract: The magnetic interaction and spin transfer via phosphorus have been investigated for the tri-*tert*-butylaminoxyl *para*-substituted triphenylphosphine oxide. For this radical unit, the conjugation existing between the π* orbital of the NO group and the phenyl π orbitals leads to an efficient delocalization of the spin from the radical to the neighboring aromatic ring. This has been confirmed by using fluid solution high-resolution EPR and solid state MAS NMR spectroscopy. The spin densities located on the atoms of the molecule could be probed since ^{1}H, ^{13}C, ^{14}N, and ^{31}P are nuclei active in NMR and EPR, and lead to a precise spin distribution map for the triradical. The experimental investigations were completed by a DFT computational study. These techniques established in particular that spin density is located at the phosphorus ($\rho = -15 \times 10^{-3}$ au), that its sign is in line with the sign alternation principle and that its magnitude is in the order of that found on the aromatic C atoms of the molecule. Surprisingly, whereas the spin distribution scheme supports ferromagnetic interactions among the radical units, the magnetic behavior found for this molecule revealed a low-spin ground state characterized by an intramolecular exchange parameter of $J = -7.55\ cm^{-1}$ as revealed by solid state susceptibility studies and low temperature EPR. The X-ray crystal structures solved at 293 and 30 K show the occurrence of a crystallographic transition resulting in an ordering of the molecular units at low temperature.

Keywords: EPR spectroscopy · magnetic properties · NMR spectroscopy · radicals · spin distribution

Introduction

It is usually considered that the knowledge of the spin density distribution for a paramagnetic compound is the ultimate information to account for the magnetic behavior exhibited by a molecule or an assembly of molecules in the crystal. For a paramagnetic compound the mixing of the SOMO (single occupied molecular orbital) with several orbitals localized on the molecular fragments may lead to the delocalization of the unpaired electron.[1] As a consequence, the spin is not exclusively located on one atom or functionality but distributed over the molecule. Starting from the core group bearing the unpaired electron, this spin delocalization over the entire molecule leads to a pattern which reflects the polarization of the σ- and π-bonding electrons. Thus, two neighboring atoms will respectively bear α spin (positive spin) and β spin (negative spin) density, and this sign alternation is spread over the whole molecule. For instance, for a molecule containing two radical units in ferromagnetic interaction, the spin polarization pattern developed on the molecular moiety linking them yields the same sign for both the radicals. On the contrary, when they are in antiferromagnetic interaction the sign of their respective spin is opposite. This spin polarization scheme which can be observed experimentally by spectroscopic techniques,[1–4] is also used as straightforward predictive tool to determine a priori the sign

[a] O. B. Borobia, Dr. P. Guionneau, Dr. J.-P. Sutter
Institut de Chimie de la Matière Condensée de Bordeaux
CNRS, Université Bordeaux 1, 87 Ave. Dr. Schweitzer
33608 Pessac (France)
Fax: (+33) 540-002-649
E-mail: jpsutter@icmcb-bordeaux.cnrs.fr

[b] Dr. H. Heise, Prof. Dr. F. H. Köhler
Anorganisch-chemisches Institut
Technische Universität München, 85747 Garching (Germany)
E-mail: F.H.Koehler@lrz.tu-muenchen.de

[c] Dr. L. Ducasse
Laboratoire de Physico-Chimie Moléculaire
Université Bordeaux 1, 33405 Talence (France)

[d] Dr. J. Vidal-Gancedo, Prof. Dr. J. Veciana
Institut de Ciència de Materials de Barcelona
Campus Universitari de Bellaterra, 08913 Cerdanyola (Spain)
E-mail: vecianaj@icmab.es

[e] Dr. S. Golhen, Dr. L. Ouahab
LCSIM UMR 6511 CNRS-Université de Rennes 1
Institut de Chimie de Rennes
35042 Rennes Cedex (France)

[f] Dr. H. Heise
New address: Max-Planck-Institute for Biophysical Chemistry
Am Fassberg 11, 37077 Göttingen (Germany)

Supporting information for this article is available on the WWW under http://www.chemeurj.org/ or from the author: Field dependence of the magnetization at 2 K, temperature dependence of the variation of the $\Delta m_s = 2$ signal between 5 and 80 K, detailed solid-state NMR data, and selected geometrical parameters for the UB3LYP/6-31g* optimized structure for compound **1**.

DOI: 10.1002/chem.200400656

of the intramolecular exchange interaction in π-conjugated organic polyradicals.[5–7]

We recently reported on a family of open-shell phosphine derivatives which were envisaged because of the possibility offered by these molecules to coordinate to transition-metal ions by the mean of the phosphine moiety and the aminoxyl radical groups.[8–13] The information gathered for a series of nitronyl nitroxide substituted phosphine derivatives established the presence of spin density at phosphorus and, more important, a spin distribution in accordance with high-spin ground states for the polyradical derivatives.[14] Unfortunately, too weak intramolecular exchange interactions due to the poor spin delocalization for nitronyl nitroxide radicals hampered the observation of the actual magnetic behavior exhibited by the molecules.

In order to gain further and conclusive information on the capability of a P atom to mediate the exchange interaction between the paramagnetic centers it bridges, we designed a molecule with an increased strength of the interaction between the spin carriers. This was achieved by enhancing the spin density located on the triphenylphosphine core and choosing a spin distribution scheme such as the C atoms bound to P bear positive spin. The molecule investigated in the present study is the tri-*tert*-butylaminoxyl substituted triphenylphosphine oxide. For this radical unit, the conjugation that exists between the π* orbital of the NO group and the phenyl π orbitals leads to an efficient delocalization of the spin from the radical on the aromatic ring. This has been confirmed by the spin distribution mapping undertaken by fluid solution high-resolution EPR[4] and NMR[1] spectroscopy which have proven to be very efficient tools in assessing the magnitude and sign of the spin density borne by the atoms of organic open-shell molecules. The spin densities located on all atoms of the molecule could be probed since all are active nuclei in NMR and EPR, that is, ^{1}H, ^{13}C, ^{14}N, and ^{31}P, and lead to a precise spin distribution map. These experimental investigations were completed by a DFT computational study. Surprisingly, whereas the spin distribution scheme supports ferromagnetic interactions among the radical units, the magnetic behavior found for this molecule revealed a low-spin ground state.

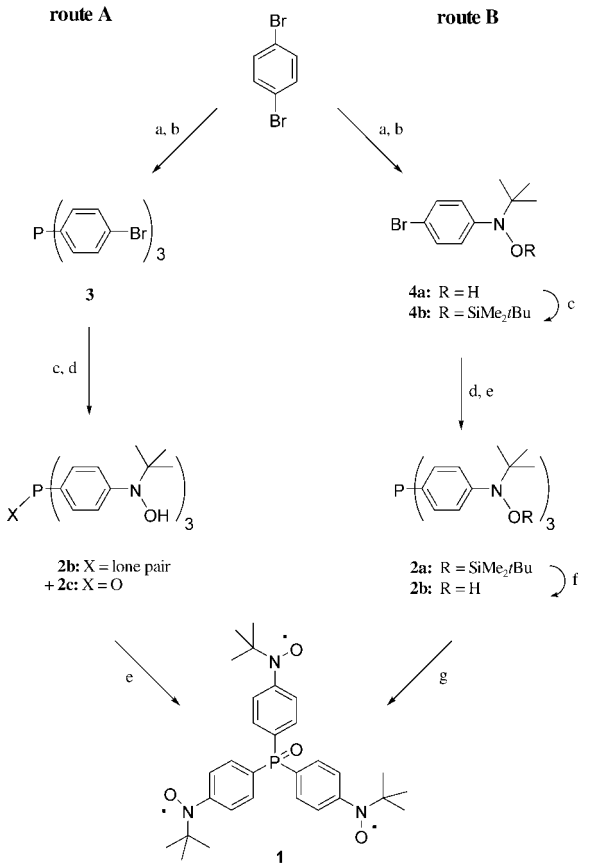

Scheme 1. Synthesis routes to triradical **1**. Route A: a) *n*BuLi; b) PCl_3, c) *n*BuLi, d) $(t\text{BuNO})_2$, e) $NaIO_4$; route B: a) *n*BuLi, b) $(t\text{BuNO})_2$, c) $ClSiMe_2t\text{Bu}$, d) *n*BuLi, e) PCl_3, f) Bu_4NF, g) $NaIO_4$.

Results

Synthesis

The triradical **1** was prepared according to the two synthesis pathways outlined in Scheme 1. Following route A, the core of the molecule was first formed from *para*-dibromobenzene and trichlorophosphine leading to tri-(4-bromophenyl)phosphine (**3**). The latter was lithiated with BuLi and treated with 2-methyl-2-nitrosopropane to give the corresponding tris(hydroxylamine). Based on ^{31}P NMR spectrum the crude reaction product appeared to be a mixture of phosphine **2b** and phosphine oxide **2c**. Triradical **1** was then obtained by oxidation with $NaIO_4$ which also converted the phosphine derivative to the corresponding phosphine oxide.

By route B, the organic fragment containing the radical precursor unit, **4a**, **b**, was first prepared from *para*-dibromobenzene and 2-methyl-2-nitrosopropane, and protected as a silane derivative. Its lithiation with *n*BuLi and subsequent reaction with PCl_3 yielded tris[p-{(*O*-*tert*-butyldimethylsilyl)-*N*-*tert*-butyl-oxylamino}phenyl]phosphine (**2a**). The conversion to the corresponding tris(hydroxylamine) **2b** was efficiently achieved with Bu_4NF in THF. Previous studies on such systems showed that it is possible to selectively obtain the radical without oxidizing the P^{III} center when Ag_2O is used as oxidant.[9,12,15] This proved not to be the case here, only a partial oxidation was observed independent of the stoichiometry considered. The oxidation was therefore conducted as in route A to obtain the triradical **1**. The overall yield with respect to PCl_3 is about 15% either by route A or B. Route B has the advantage that the products of each step can be purified.

X-ray crystal structure

Single crystals suitable for X-ray crystallographic analysis were obtained by slow diffusion of Et_2O to a solution of

compound **1** in $CHCl_3$. The structure was investigated at 293 and 30 K, the crystallographic parameters are given in Table 1. A view of the molecular structure at 293 K is depicted in Figure 1 with selected geometrical features. The

Table 1. Crystal and experimental data for triradical **1** at 293 and 30 K.

Triradical **1**	$T=293$ K	$T=30$ K
formula	$C_{30}H_{39}N_3O_4P$	$C_{30}H_{39}N_3O_4P$
M_w	536.61	536.27
crystal system	triclinic	trigonal
space group	$P1$	$P3$
λ [Å]	0.71073	0.71069
a [Å]	6.0984(3)	20.799(5)
b [Å]	12.3080(7)	20.799(5)
c [Å]	12.3112(7)	6.005(5)
α [°]	117.363(3)	90.0
β [°]	101.582(3)	90.0
γ [°]	96.494(3)	120.0
V [Å^3]	781.19(7)	2250(2)
Z	1	3
ρ [g cm^3]	1.141	1.188
$2\theta_{max}$ [°]	26.0	23.4
μ [mm^{-1}]	0.124	0.129
reflections		
measured	4866	9713
independent	4866	3876
used in refinement	4866	3876
parameters	343	344
$R1$	0.047	0.077
$wR2$	0.1193	0.1738
residue [e$^-$·Å^{-3}]	0.19/−0.18	0.45/−0.38

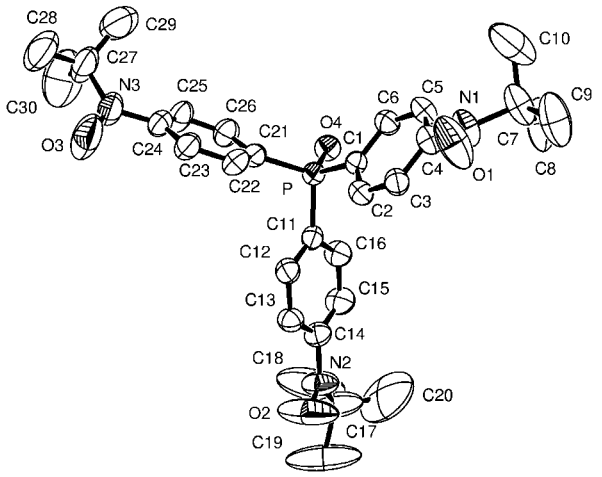

Figure 1. ORTEP drawing of compound **1** at 293 K with thermal ellipsoid plots at 30% probability level. The hydrogen atoms are omitted for clarity. Selected distances [Å] and angles [°]: O1−N1 1.271(3), O2−N2 1.260(4), O3−N3 1.272(4), N1−C4 1.420(4), N1−C7 1.500(5), N2−C14 1.409(4), N2−C17 1.475(5), N3−C24 1.431(4), N3−C27 1.474(5), P−O4 1.490(2), P−C21 1.802(3), P−C11 1.805(3), P−C1 1.805(3), O1−O2 9.864(6), O2−O3 9.896(5), O1−O3 9.975(5); O1-N1-C4 115.9(2), O2-N2-C14 116.3(3), O3-N3-C24 115.7(3), O4-P-C21 111.63(12), O4-P-C11 111.94(12), O4-P-C1 111.82(12), O1-N1-C4-C3 27.3(4), O2-N2-C14-C13 16.8(6), O3-N3-C24-C23 33.0(5).

crystal structure confirms the formulation of compound **1** as a phosphine oxide derivative with the three *t*BuNO units in *para* position of the phenyl rings. At room temperature, the P−O bond length (1.490(2) Å) is in the order of that found for other radical substituted phosphine oxide derivatives.[8,16] and the O-P-C angles close to 112° do not reflect any steric constraint in the molecule. The phosphorus atom is located at 0.670(2) Å out of the plane defined by C1-C11-C21, the corresponding phenyl rings are tilted from this plan by 73.5(1), 72.6(2) and 72.5(2)°, respectively. The C−C bonds lengths for the phenyl groups are in the range [1.381(4)–1.373(5) Å] and those connecting the aminoxyl N atoms to the aromatic rings are found between 1.409(4) and 1.431(4) Å excluding a conceivable quinonoid structure for **1**. The dihedral angles of the aminoxyl units with the phenyl groups they are linked to are 31.1(2), 16.8(3) and 34.5(2)°. Finally, the intramolecular separations between the aminoxyl groups taken as the O···O distances are 9.863(6), 9.896(6), and 9.975(6) Å. These features reveal that each Ph-NO(*t*Bu) moiety has slightly different geometric characteristics. However, the later appear in good agreement with those found usually.[11,12,17,18]

Figure 2 shows the crystalline organization in the *bc* and *ac* planes. The molecular stacking can be described as a superposition of layers along the *a* axes. In these layers, all the

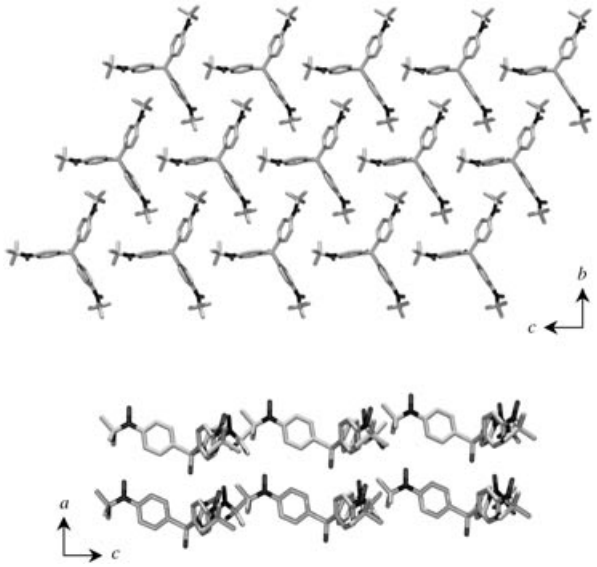

Figure 2. Projection of the crystal packing for triradical **1** at 293 K along *a* (top) and along *b* axis (bottom).

O atoms of the aminoxyl groups are pointing in the same direction but in an opposite direction to that of the P−O bond, and are almost parallel to each other. The shortest interlayer distance involves the PO unit and a phenyl group, O4···H22, with 2.490(2) Å, and the shortest intermolecular separation within a layer is found for H9b(*t*Bu) and H13(Ph) with 2.54 Å. As far as the aminoxyl units are concerned, the shortest intermolecular separations are found for O1···H5(*t*Bu), 2.678(4) Å, O2···H15(Ph), 2.652(5) Å, and O3···H25(Ph), 2.644(3) Å, and the minimum intermolecular separation between two NO groups is 5.82 Å.

A view of the molecular structure of the molecule at 30 K is depicted in Figure 3a. Compared with the structure at 293 K, a higher symmetry is observed at low temperature, the space group is now P3. It can be noticed that both high and low temperature crystal packings are chiral. The unit cell contains three independent molecules, each located on a C3 symmetry axis. As a result, at 30 K the three Ph-NO(*t*Bu) moieties of a molecule are strictly equivalent, which is not the case within the 293 K structure (Figure 3b).

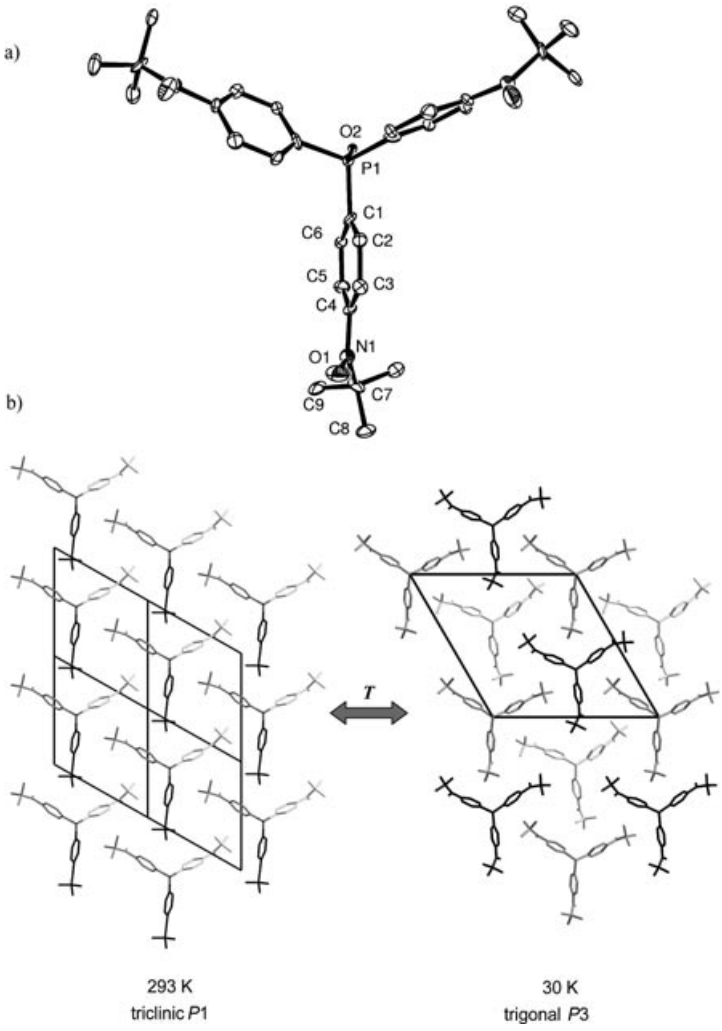

Figure 3. a) ORTEP drawing of triradical **1** at 30 K with thermal ellipsoid plots at 30 % probability level. The hydrogen atoms are omitted for clarity. Selected distances [Å] and angles [°]: Molecule 1: O1−N1 1.281(8), N1−C4 1.451(8), N1−C7 1.514(8), P1−O2 1.497(8), P1−C1 1.823(8), O1···O1 9.957(8), O1-N1-C4 115.7(1), C4-N1-C7 124.3(1), O2-P1-C1 111.7(1), C1-P1-C1 107.1(1), C3-C4-N1-O1 25.0(1); molecule 2: O4−N2 1.293(8), N2−C10 1.425(8), N2−C16 1.523(8), P2−O3 1.489(8), P2−C13 1.812(8), O4···O4 10.190(9), O4-N2-C10 117.0(1), C10-N2-C16 124.6(1), O3-P2-C13 111.4(1), C13-P2-C13 107.5(1), C11-C10-N2-O4 37.5(5); molecule 3: O6−N3 1.275(8), N3−C23 1.405(8), N3−C26 1.513(8), P3−O5 1.479(8), P3−C20 1.792(8); O6···O6 9.810(9), O6-N3-C23 116.8(1), C23-N3-C26 126.4(1), O5-P3-C20 111.8(1), C20-P3-C20 107.0(5), C24-C23-N3-O6 5.9(1). b) Comparison of the crystal packing and the unit cells at 293 and 30 K. At a given temperature, the geometry of the molecular parts drawn with the same color are strictly identical for symmetry reasons.

The three independent molecules of the unit cell display a dihedral angle between the aminoxyl units and the phenyl groups of 5.9, 25.0 and 37.5°, respectively. The other interatomic distances and angles are close to those observed at 293 K. The organization of the molecules in layers is also maintained at 30 K, the shortest separations involving the aminoxyl units being in the order of those found at 293 K with O1···H5(*t*Bu), 2.529(5) Å, O4···H15(Ph), 2.671(5) Å, and O6···H27(*t*Bu), 2.644(6) Å. The crystallographic transition is then mainly associated with an ordering of the molecular units which, at 30 K, have a three-fold axis passing through the central phosphorus atom. As a general remark, it can be noted that structural rearrangements of the crystal lattices when cooling from room to cryogenic temperatures are often observed for organic radicals and may have significant incidence on the magnetic behavior exhibited by these species.[19–22]

Spin distribution mapping

The spin distribution mapping for triradical **1** was undertaken by fluid solution high-resolution EPR and solid state MAS NMR spectroscopies as well as by DFT calculations.

High-resolution isotropic EPR: When performed in dilute fluid solutions under high-resolution conditions, EPR measurements provide precise isotropic hyperfine coupling constants for nuclei with both large and small spin densities.[4] The value of the hyperfine coupling observed by EPR is directly related to the absolute spin density on the considered nuclei (see below). The X-band EPR spectrum of compound **1** was recorded in degassed CH_2Cl_2 solutions ($<10^{-4}$ M). The spectrum obtained at 295 K is centered at $g=2.0056$ and apparently consists of eight lines equally spaced by 3.75 G.

Figure 4 shows the spectrum together with the simulated signal. This simulation required to consider a linewidth of 0.78 G and isotropic hyperfine coupling constants (hfcc) with three equivalent N nuclei of the aminoxyl units along with the hfcc values with the central phosphorus atom and with six equivalent H atoms in positions 2/6 and six in positions 3/5 of the phenyl groups. The value found for the hfcc with the N atom, $a_N=3.80(1)$ G, is, as expected, one third of the related constant found for the mono-radical derivative ($a_N=11.6$ G).[15] The same result was found for the hfcc values with the aromatic H atoms in 2/6 and 3/5 positions with 0.7(1) and 0.29(5) G, respectively, while the corresponding values for the mono-radical derivative are 2.15 and 0.86 G.[15] By contrast, the hfcc with the P atom for compound **1**, $a_P=3.30(1)$ G, remains the same as for the mono-radical derivative ($a_P=3.284$ G). This result can be ascribed to the particular position of the P atom at the center of this trigonal molecule which shares the three singly-occupied molecular orbital (SOMO) of this triradical. The very close values for a_N and a_P lead to an overlapping of the central lines and indeed yield a spectrum apparently composed of only eight lines (see stick diagram in Figure 4). The further splitting of these main lines by the coupling with the H

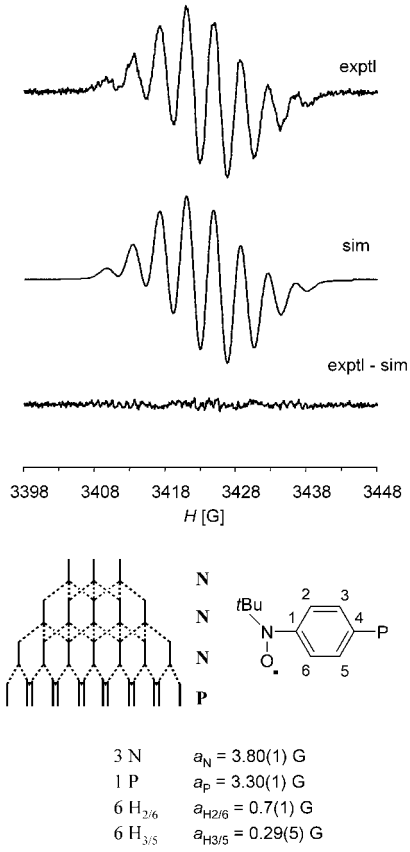

Figure 4. Top: Experimental and simulated EPR spectra of triradical **1** in fluid solution. Bottom: Stick diagram showing the eight overlapping lines along with the numbering scheme for **1**.

atoms is not resolved, instead the observed signals are rather broad with an apparent linewidth of $\Delta H_{1/2} = 2$ G. The fact that the coupling with the protons is not resolved is probably due to the small hfcc values of H atoms which lead to an overlap of the signals. In addition, electron–electron dipolar interactions, which may result from the not so large inter-radical separation within the molecule broaden the lines and hence contribute to an additional overlap. Such a line broadening due to dipolar interactions, when going from a mono-radical to a triradical derivative, was observed for related series of polyradical compounds.[14]

The high-resolution spectrum obtained for triradical **1** in fluid solution suggests that the spin density is spread over the core of the molecule. Moreover, the observation of a coupling with the P clearly indicates that spin density is located on this atom. To gather a more precise information on the spin distribution for this compound we applied solid state MAS NMR spectroscopy.

Spin-density distribution by ^{1}H, ^{13}C and ^{31}P MAS NMR spectroscopy: Solid state magic angle spinning NMR spectroscopy has recently been shown to be a powerful and simple alternative to polarized neutron diffraction for mapping the distribution of the spin density in paramagnetic molecular and supramolecular solids.[23–25] This technique provides information on both the value and the sign of the spin density of the magnetically active nuclei. Moreover, it appeared ideally suited for the compound envisaged in the present study since all atoms of the molecular fragment linking the radical units are nucleus active in NMR, that is, ^{1}H, ^{13}C, and ^{31}P.

The MAS NMR spectra of the solid compound **1** are depicted in Figure 5. The ^{1}H spectrum shows three isotropic signals that are assigned to the triradical. The methyl protons of the *tert*-butyl groups appear at −0.13 ppm, and the protons in position 3/5 and 2/6 of the phenyl groups are seen at 70 and −138 ppm, respectively. An additional peak near −244 ppm is due to nickelocene which has been used for internal calibration of the temperature in much the same way as described previously.[26] The ^{13}C NMR signals (middle spectrum) for the triradical with negative shifts are assigned to the *tert*-butyl quaternary C_α atoms and to the phenyl C in position 3/5 at −1211 and −535 ppm, respectively. The sharp signal at 1066 ppm is assigned to the methyl C_β atoms while the signal for the carbon atoms in position 4 and 2/6 appear as shoulders of the methyl signal. The latter signal shifts had to be estimated and are considered to have

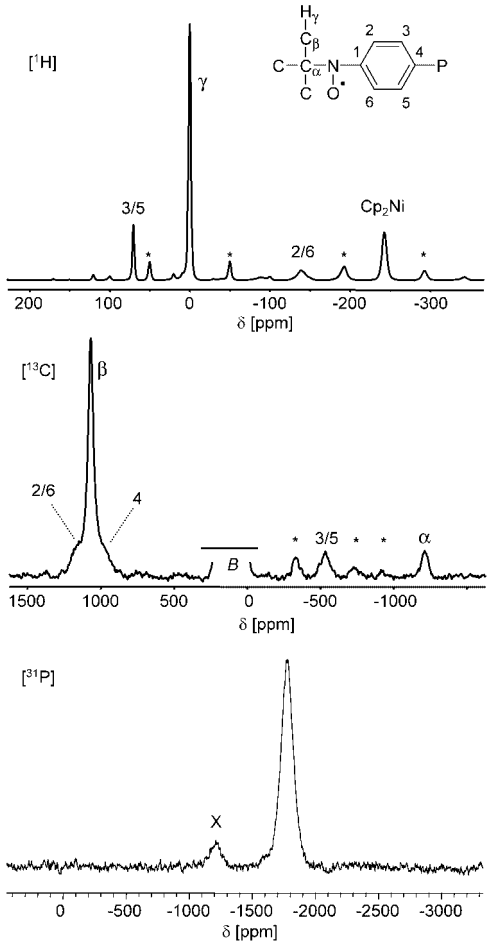

Figure 5. ^{1}H, ^{13}C, and ^{31}P MAS NMR spectra from top to bottom for triradical **1** (T = 310.8 K, spinning rate: 15 kHz). Spinning side-bands are marked by asterisks. The signal of Cp_2Ni was used as internal temperature standard; X = impurity (probably the diradical derivative).

an error limit of ± 30 ppm. We were unable to detect the signal of C1 probably because of its proximity to the spin source, which entails unfavorable relaxation.[1] Finally, in the ^{31}P MAS NMR spectrum a signal was found at -1781 ppm.

Conversion of the experimental signal shifts into the contact shifts, δ^{con}, (see Supporting Information) and further into the hyperfine coupling constants, a_X, of the nucleus X by using Equation (1) gave the data collected in Table 2. In Equation (1), γ_X is the nuclear gyromagnetic ratio, h and k are the Planck and Boltzmann constant, T is the absolute temperature, g_X is the isotropic g factor of nucleus X, β_E is the Bohr magneton, and S is the spin quantum number. The contact shifts were also converted into the spin densities, ρ_X at the nucleus X by means of Equation (2) where μ_0 is the vacuum permeability and a_0 the Bohr radius, while the other symbols have been mentioned with Equation (1). The absolute value of spin density at a nucleus X can also be deduced from the experimental hyperfine coupling constant obtained by EPR, the conversion is done with the Fermi equation given Equation (3), where β_X is the nuclear magnetic moment. The spin densities derived from MAS NMR data as well as those obtained from EPR data are given in Table 2.

$$a_X = \frac{3\gamma_X hkT}{g_x^2\beta_E^2 S(S+1)}\delta_T^{con}(X) \quad (1)$$

$$\rho_X = \frac{9kT\,a_0^3}{\mu_0 g_x^2\beta_E^2(S+1)}\delta_T^{con}(X) \quad (2)$$

$$\rho_X = \frac{3\,S}{\mu_0 g_X\beta_X}a_X \quad (3)$$

The qualitative and quantitative data concerning the spin born by the atoms of the molecule permit to draw a pattern of the spin distribution where the sign of the spin alternates from one atom to the other, as shown schematically in Figure 6.

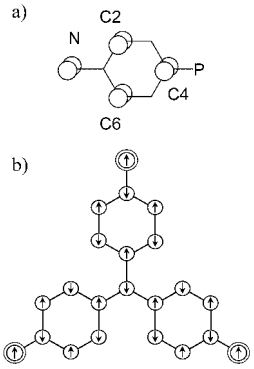

Figure 6. a) Delocalization of the positive spin density as a result of the mixing of the π^* orbital of a NO unit with the aromatic π-orbitals; b) Spin polarization map for triradical **1** (positive spin $=\uparrow$ and negative spin $=\downarrow$).

Magnetic properties

Solid-state behavior: The magnetic properties of triradical **1** were investigated on a polycrystalline sample in the temperature domain 2 to 300 K. The temperature dependence of the molar magnetic susceptibility, χ_M, is given in Figure 7 as a plot of $\chi_M T$ versus T. At 300 K the value for $\chi_M T$ is 1.10 $cm^3 K mol^{-1}$, close to the 1.125 $cm^3 K mol^{-1}$ expected for three non-interacting $S = {}^1/_2$ spins, and steadily decreases as the temperature is lowered to reach 0.28 $cm^3 K mol^{-1}$ at 2 K. Such a behavior is indicative for overall antiferromagnetic interactions among the spin carriers. In order to reveal possible contributions arising from intermolecular exchange interactions, a diluted sample of **1** (6% mass) in polyvinyl chloride (PVC) was measured in the same conditions. The temperature dependence of $\chi_M T$ (Figure 7) shows however only slight differences with respect to the crystalline sample in the low temperature domain. This suggests that the main contribution to the magnetic behavior arises from intramolecular exchange and that intermolecular interactions are

Table 2. Contact shifts (δ^{con} in ppm), hyperfine coupling constants (a in G), and spin densities (ρ in au $\times 10^{-3}$) obtained from high-resolution EPR, solid-state NMR and from DFT calculations.

	EPR[a]		NMR[b]				DFT	
	$\lvert a\rvert$	$\lvert\rho\rvert$	δ_{311}^{exptl}	δ_{298}^{com}	a [G]	ρ	ρ_{HS}[e]	ρ_{HS}[f]
H2/6	0.7	1.34[d]	−138	−152	−2.03	−1.28	−6	−6
H3/5	0.29	0.55[d]	70	65	0.87	0.55	2	3
Hγ	[c]		−0.13	−1.4	−0.019	−0.01	15/0/16[g]	17/0/17[g]
C1	[c]		[c]	[c]	[c]		−100	−136
C2/6	[c]		1055	967	3.26	8.1	124	149
C3/5	[c]		−535	−696	−2.35	−5.86	−67	−59
C4	[c]		945	846	2.85	7.1	126	143
Cα	[c]		−1211	−1325	−4.47	−11.15	−29	−27
Cβ	[c]		1066	1087	3.66	9.15		
P	3.30	15.31[d]	−1781	−1889	−10.26	−15.89	4	25
O2	[c]		[c]		[c]		4	0
N1	3.80	98.9[d]	[c]		[c]		339	491
O1	[c]		[c]		[c]		519	353

[a] Absolute values of the hfcc values obtained in CH_2Cl_2 at 293 K. [b] For details see Experimental Section and Supporting Information. [c] Not observed. [d] Obtained from Equation (3) by using three times the observed hfcc values. [e] By using the UB3LYP/6-31g* approach. [f] By using the UB3LYP/6-31+g* approach. [g] Spin densities on the H of the Me groups.

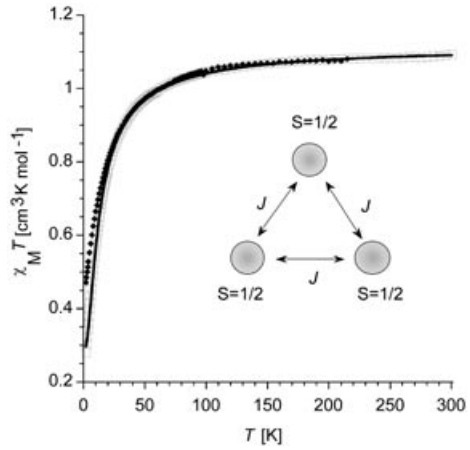

Figure 7. Experimental (□) and calculated (——) $\chi_M T$ versus T behavior for compound **1**, best fit was obtained for $J = -7.55\,cm^{-1}$ (see text). $\chi_M T$ behavior (◆) for diluted solid solution of triradical in PVC.

weak. Actually, there are intermolecular contacts as short as about 2.6 Å, but in all cases the spin density of at least one engaged nucleus is very small (Table 2).

$$\chi_M T = \frac{Ng^2\beta^2 T}{4kTF - zJ'} \quad \text{where } F = \frac{1+1\exp(\frac{3J}{2kT})}{1+5\exp(\frac{3J}{2kT})} \qquad (4)$$

The low temperature X-ray structure revealed the molecules to be highly symmetrical, therefore the magnetic behavior for triradical **1** was analyzed with a model considering three equivalent $S = {}^1/_2$ spin units located at the corners of an equilateral triangle, that is, with equivalent exchange interactions among them. The spin Hamiltonian appropriate to this situation is given by $H = -J(\hat{S}_1\cdot\hat{S}_2+\hat{S}_2\cdot\hat{S}_3+\hat{S}_3\cdot\hat{S}_1)$ where J is the exchange parameter. A rigorous description of the system would require to consider three of such interactions because the asymmetric crystal unit contains three slightly different molecules. But their respective intramolecular interaction are anticipated to be very similar and, therefore, in order to avoid over-parameterization the system was considered formed by a single type of molecule. The expression of $\chi_M T$ used to analyze the magnetic behavior of **1** is given in Equation (4) where N denotes Avogadro's number, the other symbols have been defined above. The weak intermolecular interactions have been considered in the mean-field approximation as zJ'. Least-squares fitting to the experimental data lead to $J = -7.55 \pm 0.06\,cm^{-1}$ and $zJ' = -1.40 \pm 0.06\,cm^{-1}$, by using $g = 2.00$ as a fixed constant. The antiferromagnetic nature of the intramolecular exchange interaction reveals that the ground doublet state, which is doubly degenerate, is more stable than the quartet state by $-3J/2 = 11.3\,cm^{-1}$. In order to confirm definitively this intramolecular antiferromagnetic interaction a frozen matrix EPR study of a diluted solution of triradical **1** in a solvent was undertaken.

Frozen matrix EPR spectroscopy: The frozen matrix was formed from a 10^{-3} M CH_2Cl_2/toluene (1:2) solution of triradical **1**. The spectrum recorded at 90 K consists in a broad symmetrical signal with non-symmetrical weak broad satellite lines centered at $g = 2.00$, as depicted in Figure 8. This

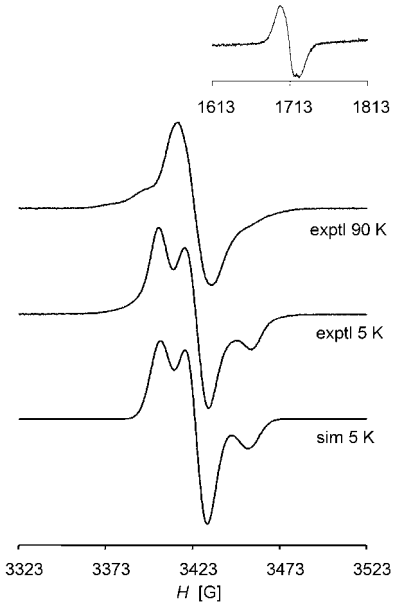

Figure 8. X-band EPR spectrum of triradical **1** in a frozen CH_2Cl_2/toluene matrix. Top: at 90 K in the $g = 2$ and $g = 4$ (insert) regions. Middle: Experimental spectrum in the $\Delta m_s = 1$ region at 5 K. Bottom: Simulated spectrum of the $\Delta m_s = 1$ signal of the doublet ground state of **1**.

set of signals corresponds to the $\Delta m_s = 1$ transitions among the sublevels of the electronic states of the triradical that are populated at this temperature, that is, assuming the same geometry as in solid state the sublevels should correspond to both the doubly degenerate ground doublet state and the first excited quartet state. A weaker signal at $g = 4$ (see insert of Figure 8) which corresponds to the $\Delta m_s = 2$ transitions and is characteristic of a quartet species, is also visible. However, the signal at $g = 6$ corresponding to the $\Delta m_s = 3$ transition which is characteristic for the quartet state of triradical species was not detected, but this forbidden transition is rarely observed.[27] The temperature dependence of the signal centered at $g = 4$ was followed between 5 and 80 K, the variation of its intensity is plotted versus $1/T$ (see Figure SI2 in the Supporting Information). For the higher temperatures the signal intensity is found to vary linearly in good agreement with a Curie law while for the lower temperature domain a downward deviation is observed confirming the occurrence of antiferromagnetic interactions among the spin carriers of the molecule. Analysis of this behavior by the model described above [Eq. (4)] yielded an intramolecular exchange parameter of $J = -3.9 \pm 0.3\,cm^{-1}$, a value in good agreement with the exchange interaction deduced for solid state behavior (Figure SI2). A worth noticing point of the EPR spectrum of triradical **1** is the evolution of the signal at the $g = 2$ region that becomes progressively asymmetric when the temperature is lowered. Thus, at 5 K it appears as three broad overlapped lines that can be simulated as a randomly oriented $S = {}^1/_2$ species

showing a coupling with one ^{14}N by using the following anisotropic parameters: $g_{xx}=2.0080$, $g_{yy}=2.0055$, $g_{zz}=2.0018$, $A_x=1.90$, $A_y=3.60$ and $A_z=25.0$ G. This result agrees with the fact that at 5 K the doublet state is the most populated state of triradical **1** and this species shows the anisotropic components of g factor and ^{14}N hyperfine coupling constant similar to those exhibited by another reported substituted *tert*-butylaminoxyl radicals.[27] This observation suggests that in frozen solution at low temperatures triradical **1** is distorted, probably due to solvent interactions, adopting a geometry in which its magnetic behavior is better described by three $S=^1/_2$ spins arranged in an isosceles triangle with two different antiferromagnetic J values for which a non degenerated doublet ground state is expected. Unfortunately, the experimental uncertainties of the intensity of $g=4$ signal does not permit to discriminate if its temperature dependence is better described by either the equilateral or the isosceles triangle models. It can be mentioned that the analyses of the experimental data by both models yielded very close exchange parameters.

Molecular modelisation of magnetic states and spin populations

The sign and magnitude of the effective magnetic coupling constant is intimately related to the balance between the direct exchange and the inter-site electronic delocalization. These constants indeed correspond to quite small differences between otherwise large total energies whose determination requires spin-dependent optimized geometries and accurate treatment of the effects of electron correlation. From comparative studies on molecular systems of reduced size, it is generally stated that the magnetic parameters extracted from Hartree–Fock (HF) theory underestimate the observed values while a density functional theory analysis leads to an overestimation of such terms, because in DFT the magnetic orbitals are excessively delocalized between the centers.[28] However, in DFT, these shortcomings can be corrected by an appropriate choice of the (hybrid) functional and thus makes such an approach quite attractive for these studies.[29,30] Mitani and co-workers compared the effective exchange integrals in *m*-phenylene coupling units. Their results show that DFT integrals are rather close to CASSCF and CASPT2 values while MPn gives a wrong sign even at fourth order.[31]

The electronic energies, the optimized geometries and the spin densities of the doublet state and of the quartet state of triradical **1** were computed by means of the density functional theory method using the B3LYP functional and the standard 6-31g* basis set. All the calculations were performed with the Gaussian03 package.[32] It is necessary to include polarisation functions in the basis set in order to account for the hypervalency of the P atom. In order to save computer time, the *tert*-butyl end groups were substituted by methyl groups.

In a first step, we checked the performance of the restricted-open shell density functional theory (ROB3LYP). The ground state is the high spin state but the calculated high spin–low spin energy difference is about 30 kcal mol^{-1}. It is thus much larger than the experimental estimate and it demonstrates that the RODFT approach does not perform efficiently. In a second step, we used the unrestricted DFT approach and we first optimized the geometry of the quartet state without any symmetry constraint and by using the RT crystal structure as a guess. The resulting energy of the optimized structure is -1619.201939 au. This geometry exhibits a C_3 symmetry (see Supporting Information for selected bond lengths, bond angles and dihedral, Table SI2). The calculated parameters are consistent with the experimental values. For example, the calculated P–O distance of 1.504 Å is quite similar to the crystal RT distance of 1.490 Å while the calculated dihedral angle O4-P1-C4-C3 of 154° agrees with the crystal value of 163°. For the doublet state, the same experimental guess induces a rather large departure from the C_3 symmetry. Instead, we used the quartet optimized geometry as a starting point and the optimized doublet state is found to be the ground state with an energy of -1619.201984 au, and this state is almost degenerate with the quartet state. The HS–LS difference is less than 0.03 kcal mol^{-1}, and it may be considered as non significant. The optimized geometries of both states are quite similar.

The eigenvalue of the total spin operator S^2 gives a good indication of the intrinsic quality of the unrestricted type calculations which in some cases may lead to spin contamination effects. For the high spin state, the S^2 eigenvalue is 3.785 (reducing to 3.751 after annihilation of the first spin contaminant) which is very close to the expected value of 3.750. For the low spin state, there exists a spin contamination because the calculated value is 1.784 (which reduces to 0.871 after annihilation of the first spin contaminant) for a theoretical value of 0.750.

The HS Mulliken spin densities are reported in Table 2 for the P and O4 atoms and for one of the three radicals. For the quartet state, each radical carries a total spin density of about 1.0. For the doublet state, two radicals exhibit a $+1.0$ density (and $\rho_i(LS) = \rho_i(HS)$, where i labels an atom of these two radicals, and the corresponding values are not reported in Table 2) and the third radical is antiferromagnetically coupled with a spin density of -1.0 (and $\rho_i(LS) = -\rho_i(HS)$, where i labels an atom of this third radical).

Discussion

The magnetic behavior of open-shell molecule-based systems is usually understood on the basis of the spin polarization Scheme displayed by the molecules. As far as conjugated hydrocarbon radicals are concerned, the spin distribution is rather well established and follows the sign alternation principle. But when a heteroatom is involved in the exchange pathway of a polyradical, the situation appears much less straightforward and very little is known on the effective implication of the heteroatom in the spin distribution. The experimental results gathered in this study unambiguously

establish the presence of spin density at the phosphorus in bridging position and show that its sign is in line with the alternation principle. More surprising however, is the discrepancy observed between the spin distribution pattern which suggests a high-spin ground state for triradical **1**, that is, an intramolecular ferromagnetic interaction, and the actual intramolecular antiferromagnetic interaction between the three radical units.

The spin density distribution found for compound **1** (Table 2) shows that the spin delocalization from the aminoxyl units onto the core of the molecule leads to the expected alternation of the sign of the spin densities among the atoms (Figure 6). The conjugation between the π*–SOMO orbital of the aminoxyl units and the π orbitals of the phenyl groups is anticipated to yield substantial positive spin on the aromatic carbon atoms in positions 2, 4 and 6, and weaker negative spin for the other positions.[1] This is indeed observed for **1** and confirmed by the opposite sign for the spin densities found on the atoms bound to these carbon centers. Thus, the H atoms 3/5 in *meta* with respect to the aminoxyl units bear positive spin whereas negative spin is found at H in position 2/6 and at the phosphorus atom. It can be noticed that the coupling constant a_P found by EPR for compound **1** is an order of magnitude larger than the one determined for the related nitronyl nitroxide triradical derivative.[14] The same trend is observed by ^{31}P NMR for the molecule which exhibits a resonance at −1781 ppm, confirming that more spin is located on P for **1** than for the corresponding nitronyl nitroxide substituted triradical. This increased spin density can be attributed to the aminoxyl radical involved here but also to the fact that for compound **1** the phosphorus is linked to phenyl C atoms bearing positive spin, that is, atoms with a higher degree of spin while for the related nitronyl nitroxide derivative the phosphorus is linked to C atoms with smaller negative spin densities. The amount of spin found at P ($-15.9.10^{-3}$ au) for **1** is in the order of the spin density found on the aromatic C atoms ($|5\times10^{-3}|$ to $|10\times10^{-3}|$ au) suggesting that the spin transfer by polarization is as efficient with the heteroatom as it is for the carbon atoms of the phenyl rings. The larger spin density found at P might be related to the fact that this atom is polarized by three C atoms bearing positive spin (C in position 4) whereas the C atoms in position 3/5 are surrounded by only two of such atoms, that is, C in positions 4 and either 2 or 6.

It is gratifying that good agreement is found between the EPR, NMR, and DFT spin density distributions. In particular that the densities on the phenyl ring are alternate with more (positive) spin at C2/6 and C4 than (negative) spin at C3/5. The calculated spin densities on these carbon atoms are, however, larger than the experimental ones. This discrepancy may be related to the use of unrestricted approach which is known to generally overestimate the difference between α-spin and β-spin populations.

The density on P deserves a particular comment. The calculated density is positive while the experimental one is negative. This sign opposition on P has been observed previously for related phosphine oxide derivatives whereas it does not apply for the corresponding phosphine compounds.[14] It is useful to refer to the recent work of Schatzschneider and Rentschler who have analyzed the spin density distributions in substituted *tert*-butyl phenyl nitroxides by using the B3YP/6-31g* approach.[33] In PO_3^{2-} nitroxide, the (non-normalized) absolute values of the spin densities are 0.6937 on NO, 0.5214 on the phenyl ring and 0.2000 on the PO_3^{2-} substituent. On the last group, the spin densities are −0.0367 on P, and 0.1161 on the O atom which is perpendicular to the plane of the phenyl ring while the two other O atoms carry a spin density of 0.0373 and 0.0199. Thus, we might expect that the negative spin density should be accounted for by using a more extended 6-31+g* basis set. We thus calculated the UB3LYP/6-31+g* energies and spin densities of triradical **1** by using the optimized UB3LYP/6-31g* geometries. The 6-31+g* HS–LS splitting does not differ a lot from its 6-31g* counterpart: the doublet is now the ground state and Δ is $-0.02\,\mathrm{kcal\,mol^{-1}}$. The corresponding spin densities of the triradical **1** in its quartet state are reported in the last column of Table 2. We found that ρ_P(6-31+g*) is even larger than ρ_P(6-31g*). To check further the dependence of the spin density on the basis set, we built a simplified model of triradical **1**, by replacing each phenyl group by a C=C bond, while keeping the same geometrical parameters. This smaller system allowed us to perform UB3LYP calculations using 6-31+g* (357 basis functions) and cc-pVTZ (724 basis functions) basis sets. In each case, the doublet is the ground state and Δ is $-0.3\,\mathrm{kcal\,mol^{-1}}$. No definite conclusion may be drawn about the spin population on the P atom because ρ_P(6-31+g*) = −0.015 while ρ_P(cc-pVTZ) = +0.014. Thus, it appears rather difficult to assess from theoretical calculations the spin density on the P atom. The size of this radical precludes any post-HF calculations (CASSCF, CASPT2, etc.) which are required to give quantitative results.

The rather efficient delocalization of the spin from the aminoxyl units onto the core of the molecule is also accounted for by the exchange interactions which exist between the spin carriers. But this magnetic behavior is in apparent contradiction with the behavior anticipated for the spin distribution scheme established for the molecule. The magnetic behaviors exhibited by both the crystalline sample and the diluted frozen sample reveal that the intramolecular radical–radical interactions are antiferromagnetic with $J = -7.55\,\mathrm{cm^{-1}}$. Based on topological rules, for a XY_3 system with spin density at Y, the simple spin polarization scheme would be expected to lead to ferromagnetic interaction. Precedents for intramolecular antiferromagnetic interaction in related poly-aminoxyl derivatives with an heteroatom (N, B or Si) in bridging position have been reported.[18,34–36] For these compounds, the antiferromagnetic interactions observed between the radical units were attributed either to a super-exchange mechanism involving a lone-pair, or to geometric considerations, that is, dihedral angles close to 90° which hamper conjugation, or to the absence of spin at the bridging atom. But these arguments do not apply for compound **1**. For the triradical the phosphorus has oxidation

state (v) and thus no lone-pair which could take part in the exchange mechanism.[14] In addition, the spin distribution mapping establishes unambiguously that spin is located at the phosphorus center. Structural features might be invoked because the molecule is not planar, the P center induces a pyramidal geometry which does not favor a good conjugation between the π system of the aromatic rings. As a consequence, spin transfer from one radical unit to another through the P is certainly hindered but does take place as clearly shown by EPR and by the degree of spin localized at P. This could lead to a pseudo-disjoint system with almost degenerated doublet and quartet states favoring the low-spin ground state.[37,38] While these considerations would explain the sign of the exchange interaction among the spin carriers they do not account for the striking contradiction that exists between the spin distribution found and the effective magnetic interaction between the radicals units. Consequently, what appears as a discrepancy may simply reveal that the observed exchange interaction is not governed by a spin polarization mechanism.

The spin system realized by triradical **1** deserves a short comment. This compound can be schematically described as consisting of three spins located at the corners of an equilateral triangle, each of which interacting equally with its two neighbors. When governed by antiferromagnetic interactions as it is the case here, there is no possibility to organize the three spins in an antiparallel orientation, a situation known as spin frustration.[39–41] In such a system, different organization for the spins of the system are possible which all lead to a magnetization at saturation lower than $M_S = 1\mu_B$ expected for a $S = {}^1/_2$ spin ground state.[42] This was also observed for the field dependence of the magnetization recorded for compound **1** at 2 K, for any field the experimental value is below the value calculated by the Brillouin function for a $S = {}^1/_2$ spin ($g = 2.00$) at this temperature (see Supporting Information). The magnetic behavior for compound **1** but also the structural features at low temperature are in agreement with a frustrated spin system. Such a characteristic makes the triradical a valuable building block for the preparation in association with paramagnetic metal ions of supramolecular magnetic coordination frameworks exhibiting properties in relation with spin frustration.

Concluding Remarks

The results gathered for triradical **1** unambiguously establish that the bridging P atom is involved in the spin distribution exhibited by the molecules. This has been confirmed by solid state MAS NMR and fluid EPR spectroscopies which proved to be powerful tools for gaining access to the spin distribution for an organic radical. The spin densities located on all atoms of the molecule could be probed, and led to a precise spin distribution map for the triradical. These techniques permitted to establish that spin density is located at the phosphorus ($\rho = -15.10^{-3}$ au) and that its sign is in line with the sign-alternation principle. Moreover, the magnitude of spin borne by the P suggests that the spin transfer by polarization is as efficient with the heteroatom as it is for the aromatic carbon atoms of the phenyl rings.

Quite surprisingly, whereas the spin distribution scheme for the triradical supports ferromagnetic interactions among the radical units, the magnetic behavior found for this molecule revealed a low-spin ground state characterized by an intramolecular exchange parameter of $J = -7.55\ cm^{-1}$. This apparent discrepancy between the found spin distribution and the effective intramolecular exchange interaction among the aminoxyl units suggests that the latter is not governed by a spin polarization mechanism.

Finally, it may be stressed that triradical **1** represents a further example of open-shell derivatives for which the structural features at low temperature are modified with respect to those found at room temperature. It underlines the importance that when a magneto-structural correlation is envisaged, the structural properties should also be studied in the temperature domain relevant for the magnetic properties.

Experimental Section

Commercially available reagents were used without further purification, except for those mentioned below which were purified as described. All solvents used in the reactions were purified by conventional methods and under inert atmosphere. Dry THF was obtained by distillation from Na/benzophenone, CH_2Cl_2 was distilled from CaH_2, MeCN was dried over P_2O_5, DMF was dried over $MgSO_4$ and distilled under vacuum, MeOH was dried over $Mg(OMe)_2$ prior to distillation. All reactions were carried out under an atmosphere of dry N_2 unless otherwise specified. 2-Methyl-2-nitrosopropane was prepared by a procedure reported in the literature.[43] Infrared spectra were recorded in the range 4000–400 cm^{-1} by using a Perkin Elmer FT-IR Paragon 1000. Elementary analysis were performed by the "Service Central d'Analyse du CNRS" at Vernaison, France. ^1H, $^{13}C\{^1H\}$ et $^{31}P\{^1H\}$ NMR spectra in solution were obtained on a Bruker ARX 300 spectrometer operating at 299.5, 75.42 and 121.42 MHz, respectively; chemical shifts (δ) are given in ppm. EPR spectra were recorded on a Bruker EMX X-band (9.4 GHz) equipped with an Oxford ESR-900 helium cryostat, the spectra simulations were done with the program WINEPR and EPRFTSM programs.[44] Magnetic measurements down to 2 K were carried out in a Quantum Design MPMS-5S SQUID susceptometer. All magnetic investigations were performed on a polycrystalline sample. The molar susceptibility was corrected for the sample holder and for the diamagnetic contribution of all atoms by using Pascal's tables.[45,46]

Synthesis of triradical 1 (route A)

Tri(4-bromophenyl)phosphine (3):[47] A solution of *p*-dibromobenzene (20 g, 84.7 mmol) in freshly distilled THF (100 mL) was added dropwise to a solution of *n*BuLi (58.28 mL, 93.1 mmol) at −78 °C. When the addition was complete, PCl_3 (2.43 mL, 84 mmol) in THF (45 mL) was introduced to the mixture at −78 °C over a period of 2 h. The reaction mixture was allowed to warm to room temperature, then filtered and the solvent was removed under reduced pressure. The yellow residue was dissolved in Et_2O (50 mL) and MeOH (30 mL) was added. The solution was stirred in order to slowly evaporated Et_2O and **3** was obtained as a white microcrystalline solid (21.79 g, 52 %). ^1H NMR ($CDCl_3$, 293 K): $\delta = 7.46$ (d, $J(H,H) = 8.17$ Hz, 6H, Ph), 7.13 (dd, $J(H,H) = 8.17$, $J(H,P) = 7.27$ Hz, 6H, Ph); $^{13}C\{^1H\}$ NMR ($CDCl_3$, 293 K): $\delta = 134.97$ (d, $J(C1,P) = 12.20$ Hz, Ph), 134.82 (d, $J(C2,P) = 20.74$ Hz, Ph), 131.68 (d, $J(C3,P) = 7.31$ Hz, Ph), 123.69 (s, Ph); $^{31}P\{^1H,^{13}C\}$ NMR ($CDCl_3$, 293 K): $\delta = -7.95$ (s); IR (KBr):

$\tilde{\nu}$ = 2986 (w), 2932 (w), 2871(w), 1568 (m), 1475 (s), 1381 (s), 1067 (s), 814 (s), 725 (s), 514 cm^{-1} (m).

Tri[*p*-(*tert*-butyl-*N*-hydroxylamino)phenyl]phosphineoxide (2c): A solution of *n*-butyllithium (11 mL, 18 mmol, 1.6 M) was added at −40 °C to a solution of tri(4-bromophenyl)phosphine (**3**; 3 g, 5.97 mmol) in Et_2O (50 mL). After the reaction mixture was allowed to warm to 0 °C, the mixture was cooled to −78 °C and a solution of 2-methyl-2-nitrosopropane (1.56 g, 8.95 mmol) in THF (10 mL) was added dropwise. Stirring was continued for 2 h at room temperature. Afterwards, a saturated aqueous solution of NH_4Cl in H_2O and Et_2O were added. The organic phase was collected and dried over $MgSO_4$ before the solvent was evaporated in vacuo. The treatment of the residue with CH_3CN gave **2** as a white powder (1.21 g, 38 %). $^{31}P\{^1H,^{13}C\}$ NMR ([D$_6$]DMSO, 293 K): δ = 27.95 (s, P^V), −9.07 (s, P^{III}); IR (KBr): $\tilde{\nu}$ = 3296 (s), 2982 (s), 2926 (s), 2876 (s), 1593 (s), 1458 (m), 1388 (m), 1189 (m), 1119 (s), 838 (m), 744 (m), 575 cm^{-1} (s).

Tri[*p*-(*tert*-butyl-*N*-oxylamino)phenyl]phosphineoxide (1): A solution of $NaIO_4$ (400 mg, 1.8 mmol) in H_2O (30 mL) was added to a solution of tri[*p*-(*tert*-butyl-*N*-hydroxylamino)phenyl]phosphineoxide (**2c**; 0.150 g, 0.288 mmol) in CH_2Cl_2 (30 mL) at 0 °C. The mixture was stirred for 15 min and the organic phase was collected, dried over $MgSO_4$ and the solvent removed to obtain a red powder. The latter was purified by chromatography over silica gel by using CH_2Cl_2/MeOH 9:1 as eluent and recrystallized from $CHCl_3/Et_2O$ to obtain **1** (0.118 g, 78 %) as red crystals. IR (KBr): $\tilde{\nu}$ = 2977 (m), 2930 (m), 2871 (w), 15781 (m), 1482 (m), 1189 (s), 1116 (F), 745 (s), 564 cm^{-1} (m); EPR (CH_2Cl_2, 293 K): g = 2.0051; 8 lines, a_N = 3.86, a_P = 3.28 G; elemental analysis calcd (%) for $C_{30}H_{39}N_3O_4P$ (536.6): C 67.14, H 7.32, N 7.83; found: C 67.32, H 7.36, N 7.86.

Synthesis of triradical 1 (route B)

Bromo-4-[*tert*-butyl-*N*-hydroxylamino]aniline (4a) (adapted from Inoue et al.[48]): *n*-Butyl lithium (39.7 mL, 63.5 mmol, 1.6 M in hexane) was added dropwise at −78 °C to a solution of *p*-dibromobenzene (15 g, 63.5 mmol) in THF (100 mL). The reaction mixture was stirred for 15 min at low temperature then gradually warmed to room temperature. The solution was again cooled to −78 °C and a solution of 2-methyl-2-nitrosopropane (6.08 g, 63 mmol) in THF (10 mL) was added slowly. The mixture was then stirred for 2 h at room temperature before a saturated aqueous solution of NH_4Cl was added followed by Et_2O. The organic layer was separated, dried over $MgSO_4$ and the solvents removed in vacuo. The resulting residue was purified by chromatography over silica gel by using hexane as eluent to obtain **4a** (10.86 g, 71 %) as a colorless oil. ^1H NMR ($CDCl_3$, 293 K): δ = 7.35 (d, J(H,H) = 8.68 Hz, 2H, Ph), 7.09 (d, J(H,H) = 8.68 Hz, 2H, Ph), 1.09 (s, 9H, *t*Bu).

Bromo-4-[*N*-*tert*-butyl-*N*-(*tert*-butyldimethylsilyloxy)]aniline (4b): The protection of the hydroxylamino group of **4a** was performed according to a method described by Corey et al.[49] To a degassed solution of **4a** (4 g, 16.3 mmol) in DMF (15 mL) were added imidazole (3.34 g, 49.1 mmol) and *tert*-butylchlorodimethylsilane (4.8 g, 32 mmol), and the reaction mixture was stirred at 50–60 °C for 24 h. After cooling and addition of H_2O (20 mL) the organic layer was extracted with hexane, dried over $MgSO_4$ and the solvent removed in vacuo. The residue was purified by chromatography over silica gel by using hexane as eluent to obtain **4b** as a colorless oil (4.85 g, 83 %). ^1H NMR spectra in agreement with the one previously reported.[50]

Tris[*p*-{(*O*-*tert*-butyldimethylsilyl)-*tert*-butyl-*N*-oxylamino}phenyl]phosphine (2a): *n*-Butyl lithium (7.2 mL, 12 mmol, 1.6 M in hexane) was added to a solution of **4b** (4.25 g, 11.9 mmol) in Et_2O (50 mL) at −78 °C. The reaction mixture was stirred for 45 min at low temperature, then a solution the PCl_3 (0.35 mL, 3.95 mL) in THF (10 mL) was added dropwise over a period of 2 h. The stirring was maintained 2 h at low temperature followed by 6 h at room temperature. After evaporation of solvents, the residue was taken off in CH_2Cl_2 (40 mL) and filtered under nitrogen to obtain a clear yellow/green solution. After removing the CH_2Cl_2 in vacuum triturating of the residue with CH_3CN yielded **2a** (1.48 g, 43 %) as a white powder. IR (KBr): $\tilde{\nu}$ = 2989 (m), 2932 (w), 2871(w), 1578 (m), 1483 (m), 1252 (s), 1173 (w), 857 (s), 743 (s), 586 cm^{-1} (m); ^1H NMR ([D$_6$]DMSO, 293 K): δ = 7.19 (dd, J(H,H) = 7.84, J(H,P) = 1.02 Hz, 6H, Ph), 7.08 (dd, J(H,H) = 7.84, J(H,P) = 7.08 Hz, 6H, Ph), 1.10 (s, 27H, *t*Bu), 0.88 (s, 27H, *t*Bu-Si), −0.12 (s, 18H, $(CH_3)_2$-Si); $^{13}C\{^1H\}$ NMR ($CDCl_3$, 293 K): δ = 154.69 (s, Ph), 132.55 (d, J(C2,P) = 20.14 Hz, Ph), 131.37 (d, J(C1,P) = 10.99 Hz, Ph), 125.15 (d, J(C3,P) = 7.32 Hz, Ph), 61.36 (s, Me_3C-Si), 61.26 (s, Me_3C-N), 26.87 (s, $(CH_3)_3$C-N), 17.95 (s, $(CH_3)_3$C-Si), −4.69 (s, $(CH_3)_2$-Si); $^{31}P\{^1H,^{13}C\}$ NMR ([D$_6$]DMSO, 293 K): δ = −8.38 (s).

Tris[*p*-(*tert*-butyl-*N*-hydroxylamino)phenyl]phosphine (2b): A solution of **2a** (2.29 g, 2.61 mmol) in THF (10 mL) was reacted under nitrogen with a 0.75 N THF solution of Bu_4NF (15 mL, 11.5 mmol) for 36 h. Afterwards, a saturated aqueous solution of NH_4Cl (50 mL) was added and the organic fraction extracted with Et_2O. The organic phase was dried over $MgSO_4$ and Et_2O partly evaporated under reduced pressure. The addition of CH_3CN under strong agitation then resulted in the formation of **2** (1.28 g, 95 %) as white powder. IR (KBr): $\tilde{\nu}$ = 3315 (F), 2981 (m), 2932 (m), 1591 (m), 1486 (s), 1200 (m), 1173 (m), 837 (s), 747 (w), 573 cm^{-1} (m); ^1H NMR ([D$_6$]DMSO, 293 K): δ = 8.33 (s, 3H, N-OH), 7.24 (dd, J(H,H) = 7.63, J(H,P) = 1.21 Hz, 6H, Ph), 7.09 (dd, J(H,H) = 7.63, J(H,P) = 6.48 Hz, 6H, Ph), 1.06 (s, 27H, *t*Bu); $^{13}C\{^1H\}$ NMR ([D$_6$]DMSO, 293 K): δ = 151.63 (s, Ph), 132.52 (d, J(C2,P) = 19.53 Hz, Ph); 132.05 (d, J(C1-P) = 9.77 Hz, Ph); 124.47 (d, J(C3,P) = 6.71 Hz, Ph), 59.79 (s, Me_3C-N), 26.29 (s, $(CH_3)_3$C-N); $^{31}P\{^1H,^{13}C\}$ NMR: δ = −8.99 (s).

Tri[*p*-(*tert*-butyl-*N*-oxylamino)phenyl]phosphineoxide (1): The oxidation of **2b** to triradical **1** was performed as described above for **2c**.

^{31}P, ^{13}C, and ^1H MAS NMR spectra: The ^{31}P, ^{13}C, and ^1H MAS NMR spectra were recorded with a Bruker MSL 300 spectrometer by using microcrystalline samples of **1**. A small amount of nickelocene has been added to **1** and used as internal temperature standard.[26,51] The powder was packed into 4 mm ZrO_2 rotors and sealed with Kel-F caps. The free induction decays were sampled after applying single 90° pulses of 2–4 μs duration with a delay time of 100–500 ms between successive scans. Data handling included exponential multiplication up to the matched filter and base line correction. The experimental signal shifts, δ^{exptl}, were determined relative to external adamantane ($\delta(^1H)$ = 2.0) and ammoniumhydrogenphosphate (($\delta(^{31}P)$ = 1.1 ppm). Contact shifts were obtained after subtracting from the experimental signal shifts, δ^{exptl}, the signal shifts, δ^{dia}, of corresponding nuclei of diamagnetic reference compounds, that is, triphenylphosphine oxide with $\delta(^{31}P)$ = 28.5 ppm, $\delta(^{13}C2/6)$ = 128 ppm, $\delta(^{13}C3/5)$ = 132 ppm, $\delta(^{13}C4)$ = 134 ppm, and $\delta(^1H)$ = 7.5 ppm for all aromatic protons, and compound **2b** was the reference compound for the proton signals of the radical moiety with $\delta(^{13}CCH_3)$ = 58 ppm, $\delta(^{13}CH_3)$ = 25 ppm, and $\delta(C,^1H_3)$ = 1.2 ppm. Note that the dipolar shift contribution can be neglected, because the *g* factor anisotropy of organic radicals is generally very small.[52] Further details are given in Table S1 of the Supporting Information.

Crystallographic studies: Small orange pyramidal shaped single crystals of approximate dimensions 0.12 × 0.12 × 0.08 mm^3 were mounted on a Bruker-Nonius four circle diffractometer equipped with a CCD camera and a graphite monochromated $Mo_{K\alpha}$ radiation source. Effective absorption correction was performed (SCALEPACK).[53] The structures were solved and the atomic parameters were refined by full-matrix least-squares method on F^2 by using the SHELX-97 package.[54] All H atoms were calculated and treated according to the riding model during refinement with isotropic displacement corresponding to the atom they are linked to.

CCDC-242664 and -242665 contain the supplementary crystallographic data for this paper. These data can be obtained free of charge via www.ccdc.cam.ac.uk/conts/retrieving.html, or from the Cambridge Crystallographic Data Centre, 12 Union Road, Cambridge CB2 1EZ, UK; fax: (+44)1223-336033; or email: deposit@ccdc.cam.ac.uk.

Acknowledgement

This work was supported by the European Union TMR Research Network ERB-FMRX-CT-98-0181 (1998–2003) entitled "*Molecular Magnet-*

ism: From Materials toward Devices". J.V. and J.V.-G. thank the Dirección General de Investigación, Spain (Project MAT2003–04699) and the Generalitat de Catalunya (Grant 2001SGR00362).

[1] F. H. Köhler, in *Magnetism: Molecules to materials*, *Vol. 1* (Eds.: J. S. Miller, M. Drillon), Wiley-VCH, Weinheim, **2001**, pp. 379–430.
[2] J. Schweizer, B. Gillon, in *Magnetic propereties of organic materials* (Ed.: P. M. Lahti), Marcel Dekker, New York, **1999**, pp. 449–473.
[3] J. Schweizer, E. Ressouche, in *Magnetism: Molecules to materials Vol. 1* (Eds.: J. S. Miller, M. Drillon), **2001**, pp. 325–355.
[4] J. Cirujeda, J. Vidal-Gancedo, O. Jürgens, F. Mota, J. J. Novoa, C. Rovira, J. Veciana, *J. Am. Chem. Soc.* **2000**, *122*, 11393–11405.
[5] H. McConnell, *J. Chem. Phys.* **1963**, *39*, 1910.
[6] P. M. Lahti, *Magnetic Properties of Organic Materials*, Marcel Dekker, New York, **1999**.
[7] K. Itoh, M. Kinoshita, *Molecular magnetism: new magnetic materials*, Gordon and Breach, Amsterdam, **2000**.
[8] C. Rancurel, J.-P. Sutter, O. Kahn, P. Guionneau, G. Bravic, D. Chasseau, *New J. Chem.* **1997**, *21*, 275–277.
[9] C. Rancurel, J.-P. Sutter, T. Le Hoerff, L. Ouahab, O. Kahn, *New J. Chem.* **1998**, *22*, 1333–1335.
[10] C. Rancurel, D. B. Leznoff, J.-P. Sutter, S. Golhen, L. Ouahab, J. Kliava, O. Kahn, *Inorg. Chem.* **1999**, *38*, 4753–4758.
[11] D. B. Leznoff, C. Rancurel, J.-P. Sutter, S. J. Rettig, M. Pink, C. Paulsen, O. Kahn, *J. Chem. Soc. Dalton Trans.* **1999**, 3593–3599.
[12] D. B. Leznoff, C. Rancurel, J.-P. Sutter, S. J. Rettig, M. Pink, O. Kahn, *Organometallics* **1999**, *18*, 5097–5102.
[13] C. Rancurel, D. B. Leznoff, J.-P. Sutter, P. Guionneau, D. Chasseau, J. Kliava, O. Kahn, *Inorg. Chem.* **2000**, *39*, 1602–1605.
[14] C. Rancurel, H. Heise, F. Köhler, U. Schatzschneider, E. Rentschler, J. Vidal-Gancedo, J. Veciana, J.-P. Sutter, *J. Phys. Chem. A* **2004**, *108*, 5903–5914.
[15] K. Torssell, *Tetrahedron* **1977**, *33*, 2287–2291.
[16] C. Rancurel, N. Daro, O. Benedi Borobia, E. Herdtweck, J.-P. Sutter, *Eur. J. Org. Chem.* **2003**, 167–171.
[17] A. W. Hanson, *Acta Crystallogr.* **1953**, *6*, 32–34.
[18] T. Itoh, K. Matsuda, H. Iwamura, K. Hori, *J. Am. Chem. Soc.* **2000**, *122*, 2567–2576.
[19] W. Fujita, K. Awaga, *Science* **1999**, *286*, 261–262.
[20] D. A. Shultz, R. M. Fico, P. D. Boyle, J. W. Kampf, *J. Am. Chem. Soc.* **2001**, *123*, 10403–10404.
[21] M. Fettouhi, E. B. Ali, E.-A. M. Ghanam, S. Golhen, L. Ouahab, N. Daro, J.-P. Sutter, *Inorg. Chem.* **2002**, *41*, 3705–3712.
[22] M. Fettouhi, E. B. Ali, M. Morsy, S. Golhen, L. Ouahab, L. B. Guennic, J.-Y. Saillard, N. Daro, J.-P. Sutter, E. Amouyal, *Inorg. Chem.* **2003**, *42*, 1316–1321.
[23] G. Maruta, S. Takeda, R. Imachi, T. Ishida, T. Nogami, K. Yamaguchi, *J. Am. Chem. Soc.* **1999**, *121*, 424–431.
[24] H. Heise, F. H. Köhler, F. Mota, J. J. Novoa, J. Veciana, *J. Am. Chem. Soc.* **1999**, *121*, 9659–9667.
[25] H. Heise, F. H. Köhler, M. Herker, W. Hiller, *J. Am. Chem. Soc.* **2002**, *124*, 10823–10832.
[26] H. Heise, F. H. Köhler, X. Xie, *J. Magn. Reson.* **2001**, *150*, 198–206.
[27] N. M. Atherton, *Principle of Electron Spin Resonance*, Ellis Horwood Prentice Hall, New York, **1993**.
[28] J. Cabrero, C. J. Calzado, D. Maynau, R. Caballol, J. P. Malrieu, *J. Phys. Chem. A* **2002**, *106*, 8146–8155.
[29] V. Baron, B. Gillon, O. Plantevin, A. Cousson, C. Mathoniere, O. Kahn, A. Grand, L. Öhrström, B. Delley, *J. Am. Chem. Soc.* **1996**, *118*, 11822–11830.
[30] T. Soda, Y. Kitagawa, T. Onishi, Y. Tanako, Y. Shigeta, H. Nagao, Y. Yoshioka, K. Yamaguchi, *Chem. Phys. Lett.* **2000**, *319*, 223–230.
[31] M. Mitani, D. Yamaki, Y. Takano, Y. Yoshioka, K. Yamaguchi, *J. Chem. Phys.* **2000**, *113*, 10486–10504.
[32] Gaussian 03, Revision Bed.04, M. J. Frisch, G. W. Trucks, H. B. Schlegel, G. E. Scuseria, M. A. Robb, J. R. Cheeseman, J. A. J. Montgomery, T. Vreven, K. N. Kudin, J. C. Burant, J. M. Millam, S. S. Iyengar, J. Tomasi, V. Barone, B. Mennucci, M. Cossi, G. Scalmani, N. Rega, G. A. Petersson, H. Nakatsuji, M. Hada, M. Ehara, K. Toyota, R. Fukuda, J. Hasegawa, M. Ishida, T. Nakajima, Y. Honda, O. Kitao, H. Nakai, M. Klene, X. Li, J. E. Knox, H. P. Hratchian, J. B. Cross, C. Adamo, J. Jaramillo, R. Gomperts, R. E. Stratmann, O. Yazyev, A. J. Austin, R. Cammi, C. Pomelli, J. W. Ochterski, P. Y. Ayala, K. Morokuma, G. A. Voth, P. Salvador, J. J. Dannenberg, V. G. Zakrzewski, S. Dapprich, A. D. Daniels, M. C. Strain, O. Farkas, D. K. Malick, A. D. Rabuck, K. Raghavachari, J. B. Foresman, J. V. Ortiz, Q. Cui, A. G. Baboul, S. Clifford, J. Cioslowski, B. B. Stefanov, G. Liu, A. Liashenko, P. Piskorz, I. Komaromi, R. L. Martin, D. J. Fox, T. Keith, Al-M. A. Laham, C. Y. Peng, A. Nanayakkara, M. Challacombe, P. M. W. Gill, B. Johnson, W. Chen, M. W. Wong, C. Gonzalez, J. A. Pople, Gaussian Inc., Pittsburgh PA, **2003**.
[33] U. Schatzschneider, E. Rentschler, *J. Mol. Struct.* **2003**, *63*, 163–168.
[34] T. Itoh, K. Matsuda, H. Iwamura, *Angew. Chem.* **1999**, *111*, 1886–1888; *Angew. Chem. Int. Ed.* **1999**, *38*, 1791–1793; .
[35] E. C. Brown, W. T. Borden, *J. Phys. Chem. A* **2002**, *106*, 2963–2969.
[36] Y. Liao, M. Baskett, P. M. Lahti, F. Palacio, *Chem. Commun.* **2002**, 252–253.
[37] T. B. Borden, E. R. Davidson, *J. Am. Chem. Soc.* **1977**, *99*, 4587–4594.
[38] T. Matsumoto, T. Ishida, N. Koga, H. Iwamura, *J. Am. Chem. Soc.* **1992**, *114*, 9952–9959.
[39] G. Toulouse, *Commun. Meth. Phys.* **1977**, *2*, 115–119.
[40] H. Y. Woo, H. So, M. T. Pope, *J. Am. Chem. Soc.* **1996**, *118*, 621–626.
[41] O. Kahn, *Chem. Phys. Lett.* **1997**, *265*, 109–114.
[42] M. F. Collins, O. A. Petrenko, *Can. J. Phys.* **1997**, *75*, 605–655.
[43] J. C. Stowel, *J. Org. Chem.* **1971**, *36*, 3055–3056.
[44] Simulation of EPR spectrum in isotropic conditions was made with Simfonia (V1.0) program (Bruker Instruments, Germany) and of EPR in frozen solution with EPRFTSM program (B. Kriste, Freie Universität Berlin, Germany).
[45] G. A. Baker, Jr., G. S. Rushbrooke, H. E. Gilbert, *Phys. Rev. A* **1964**, *135*, 1272–1277.
[46] O. Kahn, *Molecular Magnetism*, VCH, New York, **1993**.
[47] H. Ravindar, H. Hemling, H. Schumann, J. Blum, *Synth. Commun.* **1992**, *22*, 841–851.
[48] K. Inoue, H. Iwamura, *Angew. Chem.* **1995**, *107*, 973–974; *Angew. Chem. Int. Ed. Engl.* **1995**, *34*, 927–928.
[49] E. J. Corey, A. Venkateswarlu, *J. Am. Chem. Soc.* **1972**, *94*, 6190–6191.
[50] P. M. Lahti, Y. Liao, M. Julier, F. Palacio, *Synth. Met.* **2001**, *122*, 485–493.
[51] F. H. Köhler, X. Xie, *Magn. Reson. Chem.* **1997**, *35*, 487–492.
[52] R. J. Kurland, R. B. McGarvey, *J. Magn. Reson.* **1970**, *2*, 286–301.
[53] Z. M. Otwinowski, W. Minor, *Processing of X-ray Diffraction Data Collected in Oscillation Mode*, *Vol. 276*, Academic Press, **1997**.
[54] G. M. Sheldrick, Program for the refinement of crystal structures, University of Göttingen (Germany), **1997**.

Received: June 28, 2004
Published online: November 11, 2004

